Consistent nucleon-nucleon potentials and three-body forces

Z. H. Li (李增花),[1] U. Lombardo,[1] H.-J. Schulze,[2] and W. Zuo (左维)[3]
[1]*INFN-LNS, Via Santa Sofia 62, I-95123 Catania, Italy*
[2]*INFN Sezione di Catania, Via Santa Sofia 64, I-95123 Catania, Italy*
[3]*Institute of Modern Physics, 730000 Lanzhou, People's Republic of China*
(Received 6 December 2007; published 31 March 2008)

We construct microscopic three-nucleon forces consistent with the Bonn and Nijmegen two-nucleon potentials, and including Δ, Roper, and nucleon-antinucleon excitations. Recent results for the choice of the meson parameters are discussed. The forces are used in Brueckner calculations and the saturation properties of nuclear matter are determined.

DOI: 10.1103/PhysRevC.77.034316 PACS number(s): 21.65.−f, 13.75.Cs, 21.30.Fe, 24.10.Cn

I. INTRODUCTION

While nowadays several very accurate nucleon-nucleon (NN) potentials are available, the theoretical status of three-nucleon forces (TBF) is much poorer. Usually (semi)phenomenological models involving at most two-pion exchange and containing several free parameters are employed in theoretical Faddeev calculations addressing nucleon-deuteron scattering [1] or Monte-Carlo calculations of light nuclei [2–4]. Furthermore, nuclear TBF are required in variational [5] or Brueckner-Hartree-Fock (BHF) [6,7] many-body calculations of nuclear matter to obtain satisfactory saturation properties. The determination of a single TBF parametrization valid for the two extreme systems, light nuclei and nuclear matter, is still an open problem [4,7].

Currently, systematic nuclear TBF are being developed within the framework of chiral perturbation theory [8]. However, this perturbative approach is intrinsically limited to "low" energies or densities and can be considered complementary to the traditional meson-exchange picture of TBF, providing information on selection of diagrams and restricting its parameters.

In this article we develop a microscopic model of TBF, first introduced in Ref. [9], which is entirely based on the meson-exchange picture of the nucleon-nucleon interaction and involves the intermediate excitation of Δ(1232), Roper(1440), and nucleon-antinucleon states by the exchange of π, ρ, σ, and ω mesons in the TBF diagrams. The meson-exchange parameters must be chosen completely consistent with a given one-boson-exchange (OBE) NN potential; i.e., the same parameters must be used in the two- and three-body forces. This model has so far been investigated [10] together with the Paris potential [11] and the Argonne V_{14} [12] and V_{18} [13] potentials, and very satisfactory results have been obtained in BHF calculations, showing that the saturation point of nuclear matter is greatly improved compared with the use of a two-body force alone [14].

However, the potentials mentioned previously are not directly based on a meson-exchange approach; they only contain convenient empirical analytical expressions motivated by such a picture. We therefore construct in this article the microscopic TBF based on true OBE meson-exchange potentials, namely, the Bonn [15,16] and Nijmegen [17] potentials, which provide directly the necessary meson-exchange parameters. Furthermore, we discuss recent developments regarding the choice of parameters not given by the two-body force, in particular the ones related to Δ and Roper excitation.

We use the resulting TBF together with the proper NN potential in BHF calculations and determine the saturation properties of symmetric nuclear matter.

The comparison with the Dirac-Brueckner-Hartree-Fock (DBHF) approximation is an additional motivation for this study. It is in fact well known [9,18] that the TBF with nucleon-antinucleon excitations provides the main relativistic effect missing in the BHF approximation. The latter appears in the DBHF approximation from the expansion of the self-energy in powers of the scalar field, as an effect of the coupling of positive- and negative-energy Dirac states. The present framework can significantly confirm the strong similarity to the DBHF approximation obtained within the BHF calculation with the Argonne V_{14} potential and the nucleon-antinucleon TBF component of Ref. [10].

II. FORMALISM AND RESULTS

We begin with a review of the theoretical framework including the full set of final analytical expressions for the different TBF components. We use the formalism developed during a long period by several authors in Refs. [9,10,19–24], namely, a microscopic model based on two-meson exchange with intermediate excitation of nucleon resonances (Δ, Roper, and nucleon-antinucleon), as sketched in Fig. 1. The meson parameters in this model are constrained to be compatible with the two-nucleon potential, where possible.

For the use in BHF calculations, this TBF is reduced to an effective, density-dependent, two-body force by averaging over the third nucleon in the medium, the average being weighted by the BHF defect function g, which takes account of the nucleon-nucleon in-medium correlations [9,14,20,21,25]:

$$\overline{V}_{ij}(\boldsymbol{r}) = \rho \int d^3 r_k \sum_{\sigma_k,\tau_k} g(r_{ik})^2 g(r_{jk})^2 V_{ijk}. \qquad (1)$$

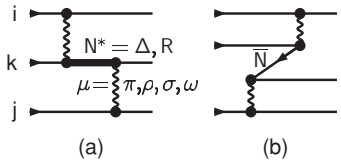

FIG. 1. Basic TBF meson-exchange diagrams.

The resulting effective two-nucleon potential has the operator structure

$$\overline{V}_{ij}(\boldsymbol{r}) = (\boldsymbol{\tau}_i \cdot \boldsymbol{\tau}_j)(\boldsymbol{\sigma}_i \cdot \boldsymbol{\sigma}_j)V_C(r) + (\boldsymbol{\sigma}_i \cdot \boldsymbol{\sigma}_j)V_S(r) + V_I(r) + S_{ij}(\hat{\boldsymbol{r}})[(\boldsymbol{\tau}_i \cdot \boldsymbol{\tau}_j)V_T(r) + V_Q(r)], \quad (2)$$

where $S_{ij}(\hat{\boldsymbol{r}}) = 3(\boldsymbol{\sigma}_i \cdot \hat{\boldsymbol{r}}_{ij})(\boldsymbol{\sigma}_j \cdot \hat{\boldsymbol{r}}_{ij}) - \boldsymbol{\sigma}_i \cdot \boldsymbol{\sigma}_j$ is the tensor operator and the five components V_O, $O = C, S, I, T, Q$, depend on the nucleon density $\rho = 2k_F^3/3\pi^2$. They are added to the bare potential in the Bethe-Goldstone equation (21) and are recalculated together with the defect function in every BHF iteration step until convergence is reached.

We next present in detail the contributions of the different two-meson exchanges in Fig. 1 to the five components of the effective TBF, Eq. (2), using the OBE parameters of the Bonn B potential.

A. $\pi\pi$ TBF

We use the classical Tuscon-Melbourne (TM) TBF of Refs. [19,21,22], which is characterized by three parameters a, b, c (the parameter d is irrelevant for the averaged TBF) and one cutoff Λ_π, apart from the coupling constant $g_{\pi NN}$. The most recent parametrization that we use is TM(99) with $a = 1.38$, $b = -2.80$, $c = 1.25$, and $\Lambda_\pi = 5.8m_\pi$ (monopole form factor) [26]. It has been argued [26,27] that a nonzero value of c is incompatible with chiral perturbation theory, but we find that the choice $c = 0$ leads to unsatisfactory saturation properties of nuclear matter (too strong attraction) and so we do not consider it further.

Furthermore, the standard TM pion cutoff $\Lambda_\pi^{\rm TM} = 5.8m_\pi \approx 800$ MeV is rather small compared to the typical πNN cutoffs employed in the two-nucleon potentials. A justification of such a small value is usually motivated by the Goldberger-Treiman discrepancy [28] or the fit of the triton binding energy involving the $\pi\pi$ TBF, neglecting, however, any other contributions to the TBF, which will be included in this article instead (see also the discussion in Refs. [22] and [24]). We therefore consider in the following also the alternative choice of using consistently the πNN cutoff of the respective potential in the TM force and present the results obtained in both cases.

The $\pi\pi$ contribution to the effective TBF reads explicitly

$$V_O^{\pi\pi}(r) = \frac{m_\pi f_\pi^2}{4\pi}\frac{1}{3}\overline{\sum_3} \times \Big[(a-2c)z_r G_x^\pi G_y^\pi + cz_r\big(F_x^\pi G_y^\pi + F_y^\pi G_x^\pi\big) + \frac{b}{3}\big(Y_x^\pi Y_y^\pi + 2P_r T_x^\pi T_y^\pi\big)\Big], \quad (O = C)$$

$$\times \Big[(a-2c)QG_x^\pi G_y^\pi + cQ\big(F_x^\pi G_y^\pi + F_y^\pi G_x^\pi\big) + \frac{b}{3}\big(P_x Y_x^\pi T_y^\pi + P_y Y_y^\pi T_x^\pi + PT_x^\pi T_y^\pi\big)\Big], \quad (O = T), \quad (3)$$

with the πNN coupling parameter $f_\pi = \frac{g_{\pi NN}}{\sqrt{4\pi}}\frac{m_\pi}{2m_N}$, where the various functions F, G, Y, and T involving the cutoff Λ_π are defined in the Appendix, and the following definitions and abbreviations are used here and in the following:

$$\overline{\sum_3} = \rho\int d^3r_3 g_x^2 g_y^2, \quad \int d^3r_3 = \frac{2\pi}{r}\int_0^\infty dx\, x\int_{|r-x|}^{r+x} dy\, y, \quad (4)$$

$$z_r = \hat{\boldsymbol{x}}\cdot\hat{\boldsymbol{y}} = \frac{x^2+y^2-r^2}{2xy}, \quad z_x = \frac{r^2+y^2-x^2}{2ry}, \quad z_y = \frac{r^2+x^2-y^2}{2rx}, \quad (5)$$

$$P_r \equiv P_2(z_r) = \frac{3z_r^2-1}{2}, \quad Q = -\frac{z_r + 3z_x z_y}{2}, \quad P = 3z_r Q - P_x - P_y. \quad (6)$$

We remark that this $\pi\pi$ TBF takes into account implicitly the effects of Δ, R, and $N\bar{N}$ excitation in the TBF diagrams in Fig. 1 [21]. In the simplest version, restricted to the excitation of a static Δ resonance (Fujita-Miyazawa model [29]), only the b term is nonzero and can be expressed by the $\pi N\Delta$ coupling parameter f_π^* given in Eq. (11):

$$a = c = 0, \quad b = -\frac{32\pi}{9}\frac{m_\pi}{m_\Delta - m_N}f_\pi^{*2}. \quad (7)$$

This represents the microscopically motivated part of the Urbana-type TBF [2–5], for example, where the coupling constant $A_{2\pi}$ is then given by [2,4]

$$A_{2\pi} = \frac{m_\pi f_\pi^2}{16\pi}\frac{b}{9} = -\frac{2}{81}\frac{(m_\pi f_\pi f_\pi^*)^2}{m_\Delta - m_N}. \quad (8)$$

The resulting $\pi\pi$ TBF, Eq. (3), at normal density $\rho = \rho_0 = 0.17$ fm^{-3} are shown [dashed (red) lines] in Fig. 2 (for $\Lambda_\pi = \Lambda_\pi^{\rm TM}$) and in Fig. 3 (for $\Lambda_\pi = \Lambda_\pi^{\rm Bonn} = 1700$ MeV). One notes clearly the importance of the cutoff, which leads to a much stronger attraction in the latter case. Using instead the TM'(99) parametrization ($a = -1, 22$, $b = -2.80$, $c = 0$) [26] (thin dashed lines) of the $\pi\pi$ TBF mentioned above, one obtains a much stronger attraction with $\Lambda_\pi^{\rm TM}$, whereas with $\Lambda_\pi^{\rm Bonn}$ the result is nearly unchanged. This behavior is due to the fact that the function F appearing in the relevant parts of Eq. (3) vanishes with increasing cutoff [see Eqs. (A3), (A16)][1]. Therefore, in the case of a large pion cutoff, the disputed c term has in any case little relevance for the averaged TBF.

[1]More precisely, it approaches the derivative of a δ function, Eq. (A20).

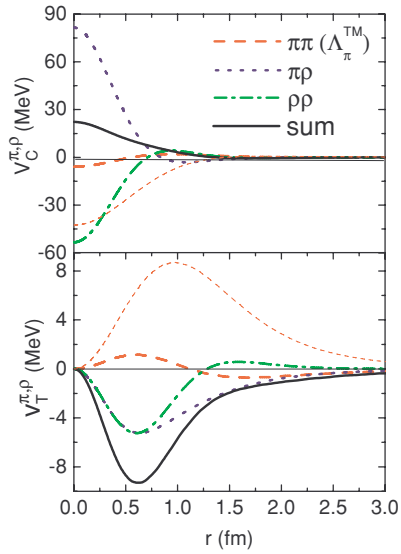

FIG. 2. (Color online) Central (upper panel) and tensor (lower panel) components of the TBF due to π and ρ exchange at normal density $\rho = \rho_0 = 0.17$ fm^{-3} and with the choice $\Lambda_\pi = \Lambda_\pi^{\rm TM} = 5.8 m_\pi$. The thin (red) dashed curves represent the case of the TM'(99) parametrization.

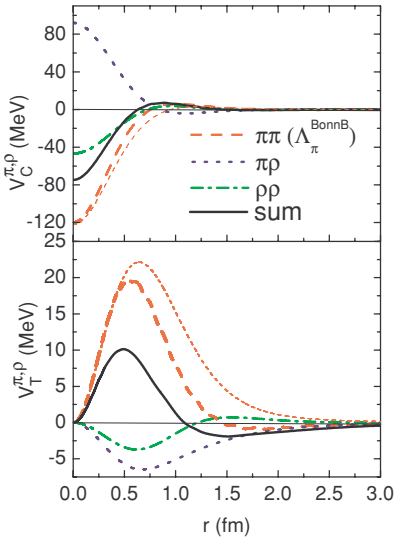

FIG. 3. (Color online) Same as Fig. 2, but with $\Lambda_\pi = \Lambda_\pi^{\rm Bonn}$.

B. $\pi\rho$ and $\rho\rho$ TBF

These TBF components are taken from Refs. [22] and correspond to the excitation of a static Δ resonance; i.e., they contain both (π, ρ)-NN and (π, ρ)-$N\Delta$ vertices:

$$V_O^{\rho\rho}(r) = -\frac{16}{81}\frac{m_\rho^2 f_\rho^2 f_\rho^{*2}}{m_\Delta - m_N}\overline{\sum_3} \times \left[2Y_x^\rho Y_y^\rho + P_r T_x^\rho T_y^\rho\right], \quad (O = C) \times \left[\frac{P}{2}T_x^\rho T_y^\rho - P_x Y_x^\rho T_y^\rho - P_y Y_y^\rho T_x^\rho\right], \quad (O = T) \tag{9}$$

and

$$V_O^{\pi\rho}(r) = -\frac{16}{81}\frac{m_\pi m_\rho f_\pi f_\pi^* f_\rho f_\rho^*}{m_\Delta - m_N}\overline{\sum_3} \times \left[Y_x^\pi Y_y^\rho - P_r T_x^\pi T_y^\rho + \{x \leftrightarrow y\}\right], \ (O = C) \times \left[\frac{P_x}{2}\left(2Y_x^\rho T_y^\pi - Y_x^\pi T_y^\rho\right) - \frac{P}{2}T_x^\pi T_y^\rho + \{x \leftrightarrow y\}\right], \ (O = T), \tag{10}$$

with the coupling parameters

$$f_\pi = \frac{g_{\pi NN}}{\sqrt{4\pi}}\frac{m_\pi}{2m_N}, \quad f_\pi^* = \frac{g_{\pi N\Delta}}{\sqrt{4\pi}}\frac{m_\pi}{2m_N} \equiv R_\pi f_\pi, \tag{11}$$

$$f_\rho = \frac{g_{\rho NN}}{\sqrt{4\pi}}\frac{m_\rho}{2m_N}(1+\kappa), \quad f_\rho^* = \frac{g_{\rho N\Delta}}{\sqrt{4\pi}}\frac{m_\rho}{2m_N}(1+\kappa) \equiv R_\rho f_\rho. \tag{12}$$

Only the (π, ρ)-NN parameters are provided by the two-body OBE force (for the Bonn B potential we have $g_{\pi NN}^2/4\pi = 14.4$, $g_{\rho NN}^2/4\pi = 0.9$, $\kappa = 6.1$), while we follow for the Δ-related parameters the prescription of the extended field-theoretical Bonn model [15] and use the quark model values $R_\pi = R_\rho = 1.8$, which is in reasonable agreement with other recent publications [30–33] involving these quantities.

Summarizing briefly the *status quo*, the $\pi N\Delta$ coupling parameter R_π approximately varies from 1.8 to 2.3. While the value $R_\pi = 1.8$ predicted by the quark model [30] was used more than three decades ago, recent fits to the experimental πp elastic-scattering database favor a larger value of $R_\pi \approx 2.3$ [31]. The Nijmegen group [32] uses $R_\pi = 2.1$ together with an exponential form factor at the $\pi N\Delta$ coupling vertex. In the Argonne V_{28} NN potential [12] with explicit Δ degrees of freedom, the value $R_\pi = 2.0$ is adopted, following the Chew-Low theory [30], which produces perfect fits to deuteron properties and np scattering below 330 MeV.

In the assessment of R_ρ there exists more uncertainty. While the Nijmegen group uses $R_\rho = 1.2$, in the triton energy spectrum analysis of Ref. [33] a value of $R_\rho = 1.85$ seems to be favored by the nucleon-nucleon potential to a great extent. However, the authors also point out that even values of $R_\rho < 0.4$ still reproduce the cross sections for both $p(n, p)n$ and $p(p, n)\Delta^{++}$ reactions very well.

In view of these uncertainties in the determination of the Δ-related parameters we follow the simple prescription of the extended field-theoretical Bonn model given above. In the BHF calculation with the Bonn B potential and the TBF presented here, it has been validated that other sets of the values of R_π and R_ρ are not able to improve further simultaneously the saturation density and the binding energy.

The $\pi\rho$ and $\rho\rho$ contributions to the TBF are also shown in Figs. 2 and 3 [dotted (blue) and dash-dotted (green) lines]. They are slightly different in both figures due to the self-consistency enforced in the BHF calculations, i.e., due to different defect functions. One notes already at this stage a strong mutual compensation between the $\pi\pi$, $\rho\rho$, and $\pi\rho$ terms, leading with $\Lambda_\pi^{\rm TM}$ (Fig. 2) to an overall repulsive central term and an attractive tensor term, both dominated by the mixed $\pi\rho$ TBF, while with $\Lambda_\pi^{\rm Bonn}$ (Fig. 3) the $\pi\pi$ component is much larger and dominates.

C. (σ, ω) TBF

These components were derived in Ref. [9] and can be divided into contributions due to $N\bar{N}$ excitation, Fig. 1(b), and due to excitation of the Roper resonance, Fig. 1(a). The former terms are given by

$$V_I^{\sigma\sigma}(r) = \left(\frac{g_{\sigma NN} m_\sigma}{4\pi}\right)^2 \frac{1}{m_N^3} \overline{\sum_3} \times \left[\left(\frac{3}{5}k_F^2 + h_x^2 + h_y^2 + 2z_r h_x h_y\right) Z_x^\sigma Z_y^\sigma - \frac{m_\sigma^2}{4}\left(Z_x^\sigma Y_y^\sigma + Z_y^\sigma Y_x^\sigma + z_r G_x^\sigma G_y^\sigma\right)\right], \quad (13)$$

where $k_F = (3\pi^2\rho/2)^{1/3}$ and $h_x = g_x'/g_x$ is the spatial derivative of the defect function,

$$V_I^{\sigma\omega}(r) = \frac{g_{\sigma NN} g_{\omega NN} m_\sigma m_\omega}{(4\pi)^2} \frac{m_\omega^2}{4m_N^3} \overline{\sum_3} \times \left[Z_x^\sigma Y_y^\omega + Z_y^\sigma Y_x^\omega\right], \quad (14)$$

and

$$V_O^{\omega\omega}(r) = \left(\frac{g_{\omega NN} m_\omega}{4\pi}\right)^2 \frac{m_\omega^2}{4m_N^3} \overline{\sum_3} \times \left[z_r G_x^\omega G_y^\omega\right], \quad (O = I),$$
$$\times \left[\frac{2z_r}{3} G_x^\omega G_y^\omega\right], \quad (O = S),$$
$$\times \left[-\frac{Q}{3} G_x^\omega G_y^\omega\right], \quad (O = Q). \quad (15)$$

We note in the $\sigma\sigma$ contribution the presence of terms proportional to $\rho^{5/3}$, which are the leading ones at high density. In fact these terms correspond roughly to the inclusion of relativistic effects within the DBHF formalism [9,18], as is discussed below.

The relevant coupling constants and form factors for the (σ, ω)-NN contributions are entirely provided by the two-nucleon OBE potential and are listed in Table I for the Bonn B potential. Figure 4 (upper panel) displays the different components of the (σ, ω)-NN TBF obtained in this manner (for the choice of $\Lambda_\pi^{\rm TM}$). One notes a fairly strong repulsion caused mainly by the $\sigma\omega$ and $\sigma\sigma$ contributions.

Coming now to the (σ, ω)-NR contributions [only to the I component in Eq. (2)], they are given by $(\mu = \sigma, \omega)$ [9]

$$W_I^{\mu\mu}(r) = \left(\frac{g_{\mu NN} g_{\mu NR}}{4\pi}\right)^2 \frac{m_\mu^2}{2m_N^3} \frac{m_N}{m_R - m_N} \boldsymbol{C}^{\mu\mu} \cdot \overline{\sum_3}$$

TABLE I. Meson-exchange parameters of the Bonn B, Nijmegen 93, and Argonne V_{18} potentials. The letter in brackets behind the form factor cutoff denotes the type of form factor: (M)onopole, (D)ipole, (E)xponential, (P)omeron, (R)oper, see the Appendix. We use the baryon masses $m_N = 938.4$ MeV, $m_\Delta = 1232$ MeV, and $m_R = 1440$ MeV.

		m (MeV)	$g^2/4\pi$	Λ (MeV)	
Bonn B	π	138	14.4	1700 (M)	$a = 1.38, b = -2.80, c = 1.25$ [TM(99)][a]
	ρ	769	0.90	1850 (D)	$\kappa = 6.1, R_\pi = R_\rho = 1.8$
	σNN[b]	550	8.94	1900 (M)	
	ωNN	783	24.5	1850 (D)	
	σNR[b]	550	0.8	2000 (R)	$\alpha = 1$
	ωNR	783	1.0	1850 (R)	$\alpha = 1$
Nijm93	π	138	13.7	1177 (E)	$a = 1.38, b = -2.80, c = 1.25$ [TM(99)][a]
	ρ	$768(0.388 \times 674 + 0.451 \times 930)$[c]	0.85	905 (E)	$\kappa = 4.1, R_\pi = 2.1, R_\rho = 1.7$
	ϵNN	$760(0.169 \times 488 + 0.613 \times 1021)$[c]	28.2	554 (E)	
	$f_0 NN$	976	12.1	554 (E)	
	PNN	938	27.3	416 (P)	
	ωNN	782	9.2	905 (E)	
	ϵNR	$760(0.169 \times 488 + 0.613 \times 1021)$[c]	1.86	2000 (R)	$\alpha = 1$
	$f_0 NR$	976	1.86	2000 (R)	$\alpha = 1$
	PNR	938	1.86	2000 (R)	$\alpha = 1$
	ωNR	782	0.6	1850 (R)	$\alpha = 1$
V_{18}	π	138	14.43	1580 (M)	$a = 1.12, b = -2.49, c = 0.98$ [TM(81)]
	ρ	776	0.55	1400 (M)	$\kappa = 6.6, R_\pi = R_\rho = 1.8$
	σNN	540	11.9	1100 (M)	
	ωNN	780	33.0	1300 (M)	
	σNR	540	2.58	1450 (R)	$\alpha = -2.35$
	ωNR	780	4.23	1550 (R)	$\alpha = -2.33$

[a]The TM(99) force is used together with a cutoff $\Lambda_\pi^{\rm TM} = 5.8 m_\pi \approx 800$ MeV or with Λ_π.
[b]This is the isospin $T = 1$ sigma meson of the Bonn B potential, which gives nearly the same results as the combined use of different $T = 0, 1$ sigma mesons [34].
[c]$m\,(c_1 \times m_1 + c_2 \times m_2)$ denotes a form factor $c_1(m_1/m)Z_1(r, m_1, \Lambda) + c_2(m_2/m)Z_1(r, m_2, \Lambda)$, Eq. (A6), see Ref. [17].

$$\times \Big[Z_x^\mu Z_y^\mu,$$
$$\Big| Z_x^\mu Z_y^\mu \left(\frac{3}{5} k_F^2 + h_x^2 + h_y^2 + 2 z_r h_x h_y \right),$$
$$\Big| Z_x^\mu \tilde{G}_y^\mu (h_y + z_r h_x) + Z_y^\mu \tilde{G}_x^\mu (h_x + z_r h_y),$$
$$\Big| Z_x^\mu \tilde{Y}_y^\mu + Z_y^\mu \tilde{Y}_x^\mu,$$
$$\Big| \tilde{G}_x^\mu \tilde{G}_y^\mu z_r \Big] \qquad (16)$$

and

$$W_I^{\sigma\omega}(r) = -\frac{g_{\sigma NN} g_{\sigma NR} g_{\omega NN} g_{\omega NR}}{(4\pi)^2} \frac{m_\sigma m_\omega}{2 m_N^3} \frac{m_N}{m_R - m_N} \boldsymbol{C}^{\sigma\omega} \cdot \sum_3$$
$$\times \Big[Z_x^\sigma Z_y^\omega,$$
$$\Big| Z_x^\sigma Z_y^\omega \left(\frac{3}{5} k_F^2 + h_x^2 + h_y^2 + 2 z_r h_x h_y \right),$$
$$\Big| \big[Z_x^\sigma \tilde{G}_y^\omega \delta(\delta - 2) - Z_x^\omega \tilde{G}_y^\sigma \delta(1 + \delta + 4\epsilon) \big] (h_y + z_r h_x),$$
$$\Big| Z_x^\sigma \tilde{Y}_y^\omega / 2 + Z_x^\omega \tilde{Y}_y^\sigma (1 + \delta - \delta^2 - 2\delta\epsilon),$$
$$\Big| \tilde{G}_x^\sigma \tilde{G}_y^\omega z_r \Big] + \{x \leftrightarrow y\} \qquad (17)$$

with $\tilde{G}_x^\mu = m_\mu G_x^\mu$, $\tilde{Y}_x^\mu = m_\mu^2 Y_x^\mu$, $\delta = m_N/m_R$, $\epsilon = m_N/(m_R - m_N) = \delta/(1-\delta)$, and

$$\boldsymbol{C}^{\sigma\sigma} = \big[-4m_N^2 |\delta^2 - 1| - 2\epsilon |(2 - \delta - \delta^2 - 2\delta\epsilon)/2| 1 - \delta \big], \qquad (18)$$

$$\boldsymbol{C}^{\omega\omega} = \big[-4m_N^2 |\delta^2 - 4\delta - 1| - 2\epsilon |(1 + \delta - \delta^2 - 2\delta\epsilon)/2| 1 + \delta \big], \qquad (19)$$

$$\boldsymbol{C}^{\sigma\omega} = \big[-4m_N^2 |\delta^2 - 3\delta - 1| 1 | 1 + \delta \big]. \qquad (20)$$

These contributions involve the coupling constants $g_{\sigma NR}$, $g_{\omega NR}$ (and the corresponding form factors), on which very little experimental or theoretical information is available. Originally [9] a special kind of form factor, Eq. (A8), was developed within a quark model of the (σ, ω)-NR vertex, but we follow here the more recent choice of simple monopole form factors of Ref. [24] with $\Lambda_{\sigma NR} = 2000$ MeV and $\Lambda_{\omega NR} = 1850$ MeV and use the coupling constants $g_{\sigma NR}^2/4\pi = 0.8$ and $g_{\omega NR}^2/4\pi = 1.0$, which optimize the saturation properties. These values lie in the range covered by independent determinations of the coupling constants, which is, however, characterized by large uncertainties:

Usually, the σNR coupling strength is estimated from the decay rate for $R \to N(\pi\pi)^{I=0}_{s\,\mathrm{wave}}$ [23,35]. In this process, the magnitude of the parameter $g_{\sigma NR}$ is tightly correlated with the mass and width of the intermediate σ meson. With a low mass of 410 MeV, one obtains a small coupling constant, $g_{\sigma NR}^2/4\pi = 0.1$ [23,36], whereas with a larger σ meson mass around 550 MeV, as indicated by Ref. [35], a value of $g_{\sigma NR}^2/4\pi = 0.56 \pm 0.35$ is used, but even a little variation of the σ meson mass strongly influences the coupling constant. In addition, the analysis of some other exclusive experiments

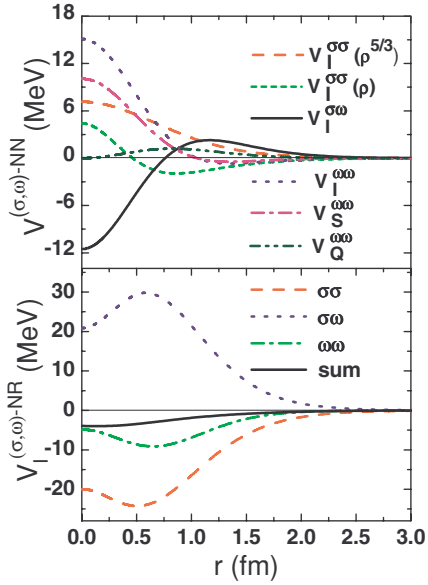

FIG. 4. (Color online) Components of the TBF due to (σ, ω)-NN (upper panel) and (σ, ω)-NR (lower panel) exchange at normal density.

discloses a very small value of $g_{\sigma NR}^2/4\pi = 0.051$ [37] or a much larger one, $g_{\sigma NR}^2/4\pi = 1.33$ [38]. In the quark model of Ref. [39] even a value of $g_{\sigma NR}^2/4\pi = 5.5$ is deduced.

Because the Roper resonance cannot directly decay into a $N\omega$ state, the ωNR coupling parameter cannot be determined directly experimentally, so that sometimes [23,24] a scaling relation, $g_{\omega NR}/g_{\omega NN} = g_{\sigma NR}/g_{\sigma NN}$, is used *ad hoc*.

The plot of the (σ, ω)-NR components in Fig. 4 (lower panel) shows that there is a very strong compensation between the $\sigma\sigma$, $\omega\omega$, and the $\sigma\omega$ contributions, which leaves an overall attractive (σ, ω)-NR TBF, which now counteracts the repulsive (σ, ω)-NN TBF shown in the upper panel of the figure. We thus observe a hierarchy of mutual cancellations of contributions of similar magnitude due to the different two-meson exchanges.

D. Mixed (π, ρ)-(σ, ω) TBF

Regarding mixed isovector-isoscalar two-meson exchanges, as discussed in Refs. [23] and [24], they do not contribute to our averaged TBF, Eq. (2), in isospin- or spin-symmetric nuclear matter due to the sum over spin and isospin of the spectator nucleon.

They do, however, slightly affect the triton binding energy in Faddeev calculations, for example, as analyzed in Refs. [23] and [24], where the compensation between the $\pi\sigma$ and $\pi\omega$ forces has been pointed out.

E. Complete TBF

Finally we display in Fig. 5 the complete set of the five components of the effective TBF, Eq. (2), at normal (upper panel) and twice normal (lower panel) nuclear density and using $\Lambda_\pi^{\mathrm{TM}}$. One notes that the only attractive component is the tensor force V_T due to (π, ρ) exchange, which is, however, compensated by the strongly repulsive central components due to both (π, ρ) and (σ, ω) exchange.

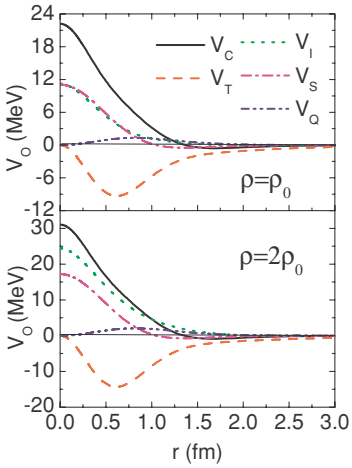

FIG. 5. (Color online) The five components of the TBF, Eq. (2), at normal density ρ_0 (upper panel) and at $2\rho_0$ (lower panel).

Comparing the results at different densities, one can see that the component I [dotted (green) curve] rises faster than the components C, T, S, and Q. While the latter ones are proportional to density, apart from the nonlinearity caused by the density-dependent defect function g in Eq. (4), the component I contains terms proportional to $\rho^{5/3}$ and thus dominates at high density, amplified by the fact that only this scalar component adds up constructively in all partial waves. This leads to an ever increasing repulsion with increasing density.

These qualitative features are confirmed in the subsequent implementation of the TBF in BHF calculations of symmetric nuclear matter, which is briefly reviewed now.

F. BHF calculations of nuclear matter

The microscopic Brueckner-Bethe-Goldstone description of nuclear matter is based on a linked cluster expansion of the energy per nucleon of nuclear matter [6]. The basic ingredient is the Brueckner reaction matrix G, which is the solution of the Bethe-Goldstone equation,

$$G[E;\rho] = V + \sum_{k_a,k_b>k_F} V \frac{|k_a k_b\rangle\langle k_a k_b|}{E - e(k_a) - e(k_b) + i\epsilon} G[E;\rho], \tag{21}$$

where $V = V_2 + V_3$ is the nucleon-nucleon interaction, in our case composed of two-nucleon potential V_2 and averaged TBF V_3 from Eq. (1), ρ is the nucleon number density, and E is the starting energy. The propagation of intermediate nucleon pairs is constrained above the Fermi momentum k_F, and the nucleon single-particle energy is

$$e(k) = e(k;\rho) = \frac{k^2}{2m} + U(k;\rho). \tag{22}$$

The BHF approximation for the single-particle potential $U(k;\rho)$ using the continuous choice prescription is

$$U(k;\rho) = \mathrm{Re} \sum_{k'\leqslant k_F} \langle kk'|G[e(k)+e(k');\rho]|kk'\rangle_a, \tag{23}$$

where the subscript a indicates antisymmetrization of the matrix elements. It has been demonstrated that the nuclear EOS can be calculated with good accuracy in the BHF two hole-line approximation with the continuous choice for the single-particle potential, because the results in this scheme are quite close to the full convergent calculations, which include also the three hole-line contributions [40].

Because of the occurrence of $U(k;\rho)$ in Eq. (22), Eqs. (21) through (23) constitute a coupled system of equations that needs to be solved self-consistently together with the computation of the defect function and the averaged TBF Eq. (1). In the BHF approximation the energy per nucleon is given by

$$\frac{B}{A} = \frac{3}{5}\frac{k_F^2}{2m} + \frac{1}{2\rho}\mathrm{Re} \sum_{k,k'\leqslant k_F} \langle kk'|G[e(k)+e(k');\rho]|kk'\rangle_a. \tag{24}$$

Technically, we have tried to obtain accurate results by enforcing the self-consistency condition Eq. (23) up to $k = 9$ fm^{-1} in momentum space and by including a large number of partial waves ($J_{\max} = 9$) in the expansion of the G matrix. The remaining angle-average approximation for Pauli operator and single-particle energies in the Bethe-Goldstone equation has been shown to introduce errors well below 1 MeV for the binding energy at saturation [41].

The left and middle panels of Fig. 6 show the saturation curves obtained within the described formalism, using the Bonn B potential together with the compatible TBF for $\Lambda_\pi^{\mathrm{TM}}$ or $\Lambda_\pi^{\mathrm{Bonn}}$, respectively. One sees that the saturation point (0.34 fm^{-3}, -22 MeV) obtained with the NN potential alone [14] is rather unrealistic, while the inclusion of TBF shifts it to (0.24 fm^{-3}, -14.7 MeV) for $\Lambda_\pi^{\mathrm{TM}}$ or to a nearly perfect (0.17 fm^{-3}, -15.9 MeV) for $\Lambda_\pi^{\mathrm{Bonn}}$. We also demonstrate the importance of the different two-meson exchange contributions to the total TBF by plotting separately the results obtained with only the $\pi\pi$ TBF, the (π,ρ) TBF, the $(\pi,\rho)+(\sigma,\omega)NN$ TBF, and the full $(\pi,\rho)+(\sigma,\omega)$ TBF. One notes clearly the cancellations between the individual terms, as pointed out in the preceding discussion.

Of course one should not expect a perfect reproduction of the empirical saturation point, in view of the numerous theoretical and numerical approximations involved in both parts of our approach, construction of the effective TBF itself, and use within the BHF approximation. The present derivation of TBF relies on the averaging prescription for the third nucleon and on static meson exchange (apart from the $\pi\pi$ contribution) involving only the lowest-mass excitations Δ and R, while the BHF approach should in fact treat three hole line and TBF corrections on an equal and consistent level, which is, however, an extremely involved problem.

It is therefore interesting to see whether the improvement of the saturation point occurs generally also with other NN potentials.

G. $\sigma\sigma$-$N\bar{N}$ TBF and Dirac-BHF approximation

To make a comparison with the DBHF approximation let us single out the contribution due to $N\bar{N}$ excitation via σ-meson exchange, Fig. 1(b). In fact, as already discussed, it appears as

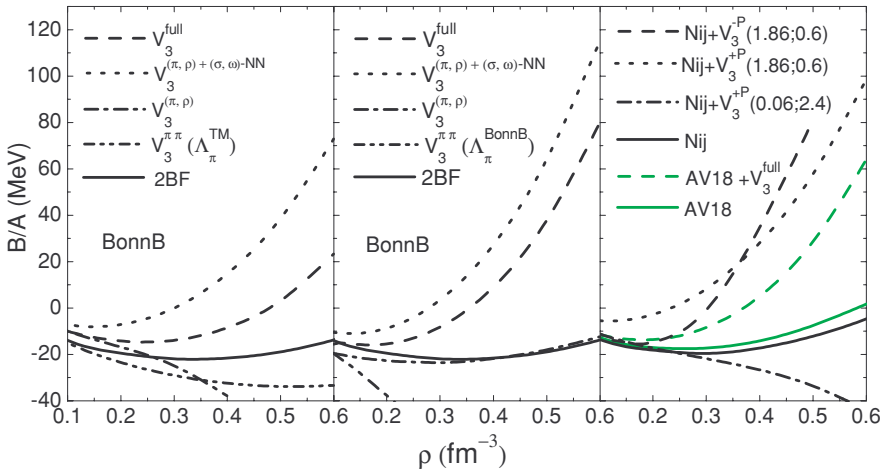

FIG. 6. (Color online) Saturation curves of symmetric nuclear matter obtained with the Bonn B potential and different contributions to the TBF using $\Lambda_\pi^{\rm TM}$ (left panel) or $\Lambda_\pi^{\rm Bonn}$ (middle panel) and with the Nijmegen 93 (black curves) or the Argonne V_{18} (green curves) potentials with and without TBF (right panel); see the discussion in the text.

a second-order term in the energy expansion to the power of the scalar field [9,18]. Accordingly, one must consider only the Hartree contribution of the $\sigma\sigma - N\bar{N}$ TBF to the EOS. The corresponding values, obtained by neglecting the correlation effects, are reported in Table II and compared with DBHF results using the Bonn B potential [15]. The agreement is quite impressive, showing that a consistent treatment of two- and three-body forces is able to give an accurate numerical support to the assumed equivalence between the two calculations. Moreover, the comparison with the BHF calculation with the full TBF (last column) can give a hint of the missing contributions in the DBHF predictions, which are necessary to give a good saturation energy.

H. Results with Argonne and Nijmegen potentials

Of the various Nijmegen NN potentials (Nijm I, Nijm II, Nijm93, Reid93) [17] only the Nijm93 is suitable for our purpose, because it is consistently based on a OBE meson-exchange picture, whereas the other potentials refit the meson-exchange parameters in each partial wave (like the CD-Bonn potential).

TABLE II. Binding energy per nucleon E/A (in MeV) in different approximations using the Bonn B potential.

k_F (fm^{-1})	BHF	DBHF	BHF + Z-diagram	BHF + TBF
0.8	−9.61	−7.02	−6.39	−6.41
0.9	−10.68	−8.58	−8.56	−8.66
1.0	−11.94	−10.06	−10.51	−11.15
1.1	−13.55	−11.18	−11.54	−13.17
1.2	−15.16	−12.35	−12.56	−14.95
1.3	−16.95	−13.35	−13.38	−15.55
1.35	−17.81	−13.35	−13.40	−15.89
1.4	−18.56	−13.53	−13.67	−15.81
1.5	−20.17	−12.15	−12.29	−14.32
1.6	−21.59	−8.46	−8.44	−10.51
1.7	−21.96	−1.61	−1.31	−3.86
1.8	−21.78	9.42	9.44	7.83
1.9	−20.34	25.26	28.43	26.18
2.0	−17.32	47.56	56.78	54.58
2.1	−12.29	77.40	94.86	90.46

A peculiarity of the Nijmegen potentials is the presence of a strong scalar NN correlation, the "Pomeron" P, which is treated like a meson exchange and compensates the very strong σ (ϵ and f_0) exchanges in this model (see Table I).

We have attempted to use the Nijm93 potential in its full complexity in our TBF. This means in particular that all the mixed meson exchanges, $\epsilon f_0, \epsilon P, f_0 P, \omega\epsilon, \omega f_0$, and ωP, must be taken into account and that the completely unknown (ϵ, f_0, P)-NR coupling constants and form factors must be specified. Nevertheless, even with these degrees of freedom we have so far been unable to construct a TBF that yields satisfactory saturation properties of nuclear matter. The problem is illustrated in the right panel of Fig. 6: Attempting to fit the saturation point without the Pomeron contribution and using the parameters $g^2_{\sigma NR}/4\pi = 1.86$ and $g^2_{\omega NR}/4\pi = 0.6$ (black dashed curve) leads to a too large incompressibility, while including the Pomeron either the saturation point is not reproduced (black dotted curve) or no saturation is obtained at all (black dash-dotted curve). The underlying reason appears to be the very large values of the ϵNN and PNN coupling constants, which in the two-nucleon case compensate each other, but in the TBF provide too strong effects.

Regarding the role of the (π, ρ)-$N\Delta$ couplings for the Nijmegen potential, increasing their values just causes an upward shift of the binding energy at the saturation point while keeping the saturation density more or less unchanged, which cannot remedy the problem illustrated above.

Finally, for completeness we list in Table I the meson-exchange parameters and plot in Fig. 6 (right panel, green curves) the saturation curves for the Argonne V_{18} potential, repeating the results of Ref. [10]. Note that in this case already on the two-body level the saturation properties are better than with the Bonn B or Nijmegen 93 potentials and that the inclusion of TBF moves the saturation point to a nearly satisfactory (0.20 fm^{-3}, −14.7 MeV).

III. CONCLUSIONS

We have constructed microscopic meson-exchange TBF incorporating Δ, Roper, and $N\bar{N}$ excitations that are completely consistent with an underlying two-nucleon OBE potential. In this work we used the Bonn B potential, in which all

relevant meson parameters are explicitly given. The remaining parameters not specified by the potential were chosen in line with independent investigations.

We have pointed out strong cancellation mechanisms taking place on different levels and which render the final resulting TBF very delicate. Nevertheless the use of the TBF together with the corresponding NN potential in nonrelativistic BHF calulations leads to a significant improvement of the saturation point of nuclear matter, which is also confirmed by calculations with other NN potentials. It thus makes sense to employ these TBF in investigations of high-density baryonic matter relevant for astrophysical applications [7,42].

Further improvements for the future regard in particular the consistent combined treatment of TBF and three-hole-line corrections within the Brueckner theory of nuclear matter.

ACKNOWLEDGMENTS

We would like to acknowledge valuable discussions with P. Grange, A. Lejeune, R. Machleidt, and J. F. Mathiot. This work has been supported in part by the Asia-Link project CN/ASIA-LINK/008(94791) of the European Commission. W. Zuo is supported in part by the National Natural Science Foundation of China (10575119), the Knowledge Innovation Project (KJCX3-SYW-N2) of the Chinese Academy of Sciences, and the Major State Basic Research Developing Program of China under No. 2007CB815004.

APPENDIX: FORM FACTORS

For reference and completeness we provide here the definitions and properties of various relevant form factors and related quantities. The numerical evaluation of the different TBF contributions involves in general the expressions

$$Z_n(r,m,\Lambda)=\frac{4\pi}{m^{(3-2n)}}\int\frac{d^3\boldsymbol{q}}{(2\pi)^3}e^{i\boldsymbol{q}\cdot\boldsymbol{r}}\frac{H(\boldsymbol{q}^2)}{(\boldsymbol{q}^2+m^2)^n} \tag{A1}$$

and their first and second spatial derivatives. Here the function H denotes the product of two meson-nucleon form factors of certain types and cutoffs. These depend on the exchanged meson (mass m) and the two-body potential chosen (see Table I). The relevant cases are as follows:

(i) Identical multipole [(S)quareroot, (M)onopole, or (D)ipole] vertices ($x\equiv mr; z\equiv\Lambda r$)

$$H(\boldsymbol{q}^2)=\left[\frac{\Lambda^2-m^2}{\Lambda^2+\boldsymbol{q}^2}\right]^i; \tag{A2}$$

$$Z_n^i(r,m,\Lambda)=\begin{cases}\frac{e^{-x}-e^{-z}}{x} & \left(\mathrm{S}:\frac{i=1}{n=1}\right)\\ \frac{e^{-x}}{x}-\left[\frac{2}{x}+\frac{z}{x}-\frac{x}{z}\right]\frac{e^{-z}}{2} & \left(\mathrm{M}:\frac{i=2}{n=1}\right)\\ \frac{x}{z}\left[1-\left(\frac{z}{x}\right)^2\right]^2\frac{e^{-z}}{2} & \left(\mathrm{M}:\frac{i=2}{n=0}\right)\\ \frac{e^{-x}}{x}-\frac{e^{-z}}{x}\left[1+\frac{z^2-x^2}{2z}\right.\\ \quad+\frac{z+1}{8z^3}(z^2-x^2)^2\\ \quad\left.+\frac{z^2+3z+3}{48z^5}(z^2-x^2)^3\right] & \left(\mathrm{D}:\frac{i=4}{n=1}\right)\end{cases} \tag{A3}$$

(ii) (E)xponential ($n=1$) and (P)omeron ($n=0$) form factors

$$H(\boldsymbol{q}^2)=\left[\exp\left(\frac{-\boldsymbol{q}^2}{2\Lambda^2}\right)\right]^2; \tag{A4}$$

$$Z_0(r,m,\Lambda)=\frac{e^{-z^2/4}}{2\sqrt{\pi}}\frac{z^3}{x^3}, \tag{A5}$$

$$Z_1(r,m,\Lambda)=\frac{e^{x^2/z^2}}{2x}\left[e^{-x}\mathrm{erfc}\left(\frac{x}{z}-\frac{z}{2}\right)-e^{x}\mathrm{erfc}\left(\frac{x}{z}+\frac{z}{2}\right)\right], \tag{A6}$$

$$Z_2(r,m,\Lambda)=-\frac{e^{x^2/z^2}}{2z}\left[e^{-x}\left(\frac{x}{z}-\frac{z}{2}\right)\mathrm{erfc}\left(\frac{x}{z}-\frac{z}{2}\right)+e^{x}\left(\frac{x}{z}+\frac{z}{2}\right)\mathrm{erfc}\left(\frac{x}{z}+\frac{z}{2}\right)\right] \tag{A7}$$

(iii) (R)oper-Nucleon form factor of Ref. [9]

(a) Together with multipole μNN-vertex

$$H(\boldsymbol{q}^2)=\left[\frac{\Lambda_N^2-m^2}{\Lambda_N^2+\boldsymbol{q}^2}\right]^i\left[\frac{\Lambda_R^2-m^2}{\Lambda_R^2+\boldsymbol{q}^2}\right]^j\left[\frac{\Lambda_R^2+\alpha\boldsymbol{q}^2}{\Lambda_R^2-\alpha m^2}\right]; \tag{A8}$$

$$Z_1^{i1}(r,m,\Lambda_N,\Lambda_R,\alpha)=Z_1^i(r,m,\Lambda_N)-\frac{(1-\alpha)\Lambda_R^2}{\Lambda_R^2-\alpha m^2}\left[\frac{\Lambda_N^2-m^2}{\Lambda_N^2-\Lambda_R^2}\right]^i\times\frac{\Lambda_R}{m}Z_1^i(r,\Lambda_R,\Lambda_N), \tag{A9}$$

$$Z_1^{12}(r,m,\Lambda_N,\Lambda_R,\alpha)=Z_1^2(r,m,\Lambda_R)-\frac{\Lambda_R^2-\alpha\Lambda_N^2}{\Lambda_R^2-\alpha m^2}\left[\frac{\Lambda_R^2-m^2}{\Lambda_R^2-\Lambda_N^2}\right]^2\times\frac{\Lambda_N}{m}Z_1^2(r,\Lambda_N,\Lambda_R), \tag{A10}$$

$$Z_1^{22}(r,m,\Lambda_N,\Lambda_R,\alpha)=\frac{\Lambda_R^2-m^2}{\Lambda_R^2-\Lambda_N^2}Z_1^{21}(r,m,\Lambda_N,\Lambda_R,\alpha)-\frac{\Lambda_N^2-m^2}{\Lambda_R^2-\Lambda_N^2}Z_1^{12}(r,m,\Lambda_N,\Lambda_R,\alpha) \tag{A11}$$

(b) Together with exponential μNN-vertex

$$H(\boldsymbol{q}^2)=\left[\exp\left(\frac{-\boldsymbol{q}^2}{2\Lambda_N^2}\right)\right]\left[\frac{\Lambda_R^2-m^2}{\Lambda_R^2+\boldsymbol{q}^2}\right]^2\left[\frac{\Lambda_R^2+\alpha\boldsymbol{q}^2}{\Lambda_R^2-\alpha m^2}\right]; \tag{A12}$$

$$Z_1(r,m,\Lambda_N,\Lambda_R,\alpha) = Z_1(r,m,\tilde{\Lambda}_N) - \frac{\Lambda_R}{m}\left[Z_1(r,\Lambda_R,\tilde{\Lambda}_N) + \frac{(1-\alpha)\left(\Lambda_R^2-m^2\right)}{\Lambda_R^2-\alpha m^2}Z_2(r,\Lambda_R,\tilde{\Lambda}_N)\right], \quad \text{(A13)}$$

$$Z_0(r,m,\Lambda_N,\Lambda_R,\alpha) = \frac{\left(\Lambda_R^2-m^2\right)^2\Lambda_R}{\left(\Lambda_R^2-\alpha m^2\right)m^3}\left[\alpha Z_1(r,\Lambda_R,\tilde{\Lambda}_N) + (1-\alpha)Z_2(r,\Lambda_R,\tilde{\Lambda}_N)\right], \quad \text{(A14)}$$

where $\tilde{\Lambda}_N = \sqrt{2}\Lambda_N$.

The μNR-vertex is a linear combination of monopole and dipole involving an additional parameter α and reduces for $\alpha = 0$ to a dipole and for $\alpha = 1$ to a monopole, which is the form factor used in Ref. [24].

All the other functions, Z, F, G, Y, T, appearing above in the various TBF components can be derived from Z_0 and Z_1 [2]:

$$Z_r^\mu = Z_1(r,m_\mu,\Lambda_\mu), \quad (\mu = \sigma,\omega \text{ only}), \quad \text{(A15)}$$

$$F_r^\mu = -\frac{1}{m_\mu}\frac{\partial}{\partial r}Z_0(r,m_\mu,\Lambda_\mu), \quad (\mu = \pi \text{ only}), \quad \text{(A16)}$$

$$G_r^\mu = -\frac{1}{m_\mu}\frac{\partial}{\partial r}Z_1(r,m_\mu,\Lambda_\mu), \quad \text{(A17)}$$

$$Y_r^\mu = \frac{1}{m_\mu^2}\left(\frac{\partial^2}{\partial r^2}+\frac{2}{r}\frac{\partial}{\partial r}\right)Z_1(r,m_\mu,\Lambda_\mu), \quad \text{(A18)}$$

$$T_r^\mu = \frac{1}{m_\mu^2}\left(\frac{\partial^2}{\partial r^2}-\frac{1}{r}\frac{\partial}{\partial r}\right)Z_1(r,m_\mu,\Lambda_\mu). \quad \text{(A19)}$$

In the case without cutoff ($\Lambda \to \infty$) these expressions reduce to the well-known Yukawa functions

$$F_r = -\frac{\partial}{\partial x}\delta^3(\boldsymbol{x}), \quad \text{(A20)}$$

$$Z_r = Y_r = \frac{e^{-x}}{x}, \quad \text{(A21)}$$

$$G_r = \frac{e^{-x}}{x}\left(1+\frac{1}{x}\right), \quad \text{(A22)}$$

$$T_r = \frac{e^{-x}}{x}\left(1+\frac{3}{x}+\frac{3}{x^2}\right), \quad \text{(A23)}$$

but the regularized results including the cutoff become lengthy and are not listed here.

[1] S. Hirenzaki, E. Oset, C. Djalali, and M. Morlet, Phys. Rev. C **61**, 044605 (2000); H. Witała, W. Glöckle, J. Golak, A. Nogga, H. Kamada, R. Skibiński, and J. Kuroś-Żolnierczuk, Phys. Rev. C **63**, 024007 (2001); J. Kuroś-Żolnierczuk, H. Witała, J. Golak, H. Kamada, A. Nogga, R. Skibiński, and W. Glöckle, Phys. Rev. C **66**, 024003 (2002).

[2] J. Carlson, V. R. Pandharipande, and R. B. Wiringa, Nucl. Phys. **A401**, 59 (1983).

[3] B. S. Pudliner, V. R. Pandharipande, J. Carlson, and R. B. Wiringa, Phys. Rev. Lett. **74**, 4396 (1995); B. S. Pudliner, V. R. Pandharipande, J. Carlson, S. C. Pieper, and R. B. Wiringa, Phys. Rev. C **56**, 1720 (1997); J. Carlson and R. Schiavilla, Rev. Mod. Phys. **70**, 743 (1998); R. B. Wiringa, S. C. Pieper, J. Carlson, and V. R. Pandharipande, Phys. Rev. C **62**, 014001 (2000); J. Carlson, J. Morales, V. R. Pandharipande, and D. G. Ravenhall, Phys. Rev. C **68**, 025802 (2003).

[4] S. C. Pieper, V. R. Pandharipande, R. B. Wiringa, and J. Carlson, Phys. Rev. C **64**, 014001 (2001).

[5] A. Akmal, V. R. Pandharipande, and D. G. Ravenhall, Phys. Rev. C **58**, 1804 (1998); J. Morales, V. R. Pandharipande, and D. G. Ravenhall, Phys. Rev. C **66**, 054308 (2002).

[6] J. P. Jeukenne, A. Lejeune, and C. Mahaux, Phys. Rep. **25C**, 83 (1976); M. Baldo, *Nuclear Methods and the Nuclear Equation of State*, International Review of Nuclear Physics (World Scientific, Singapore, 1999), Vol. 8.

[7] X. R. Zhou, G. F. Burgio, U. Lombardo, H.-J. Schulze, and W. Zuo, Phys. Rev. C **69**, 018801 (2004).

[8] E. Epelbaum, A. Nogga, W. Glöckle, H. Kamada, Ulf-G. Meissner, and H. Witała, Phys. Rev. C **66**, 064001 (2002); R. Machleidt and D. R. Entem, J. Phys. G **31**, S1235 (2005); U.-G. Meissner, Eur. Phys. J. A **31**, 397 (2007).

[9] P. Grangé, A. Lejeune, M. Martzolff, and J.-F. Mathiot, Phys. Rev. C **40**, 1040 (1989).

[10] W. Zuo, A. Lejeune, U. Lombardo, and J.-F. Mathiot, Nucl. Phys. **A706**, 418 (2002); Eur. Phys. J. A **14**, 469 (2002).

[11] M. Lacombe, B. Loiseau, J. M. Richard, R. Vinh Mau, J. Conte, P. Pirés, and R. de Tourreil, Phys. Rev. C **21**, 861 (1980).

[12] R. B. Wiringa, R. A. Smith, and T. L. Ainsworth, Phys. Rev. C **29**, 1207 (1984).

[13] R. B. Wiringa, V. G. J. Stoks, and R. Schiavilla, Phys. Rev. C **51**, 38 (1995).

[14] Z. H. Li, U. Lombardo, H.-J. Schulze, W. Zuo, L. W. Chen, and H. R. Ma, Phys. Rev. C **74**, 047304 (2006).

[15] R. Machleidt, K. Holinde, and Ch. Elster, Phys. Rep. **149**, 1 (1987); R. Machleidt, Adv. Nucl. Phys. **19**, 189 (1989); R. Brockmann and R. Machleidt, Phys. Rev. C **42**, 1965 (1990).

[16] R. Machleidt, Phys. Rev. C **63**, 024001 (2001).

[17] M. M. Nagels, T. A. Rijken, and J. J. de Swart, Phys. Rev. D **17**, 768 (1978); V. G. J. Stoks, R. A. M. Klomp, C. P. F. Terheggen, and J. J. de Swart, Phys. Rev. C **49**, 2950 (1994).

[18] G. E. Brown, W. Weise, G. Baym, and J. Speth, Comments Nucl. Part. Phys. **17**, 39 (1987).

[19] B. A. Loiseau, Y. Nogami, and C. K. Ross, Nucl. Phys. **A165**, 601 (1971).

[20] B. H. J. McKellar and R. Rajaraman, Phys. Rev. C **3**, 1877 (1971); D. W. E. Blatt and B. H. J. McKellar, Phys. Rev. C **11**, 614 (1975).

[21] S. A. Coon, M. D. Scadron, P. C. McNamee, B. R. Barrett, D. W. E. Blatt, and B. H. J. McKellar, Nucl. Phys. **A317**, 242 (1979); S. A. Coon and W. Glöckle, Phys. Rev. C **23**, 1790 (1981).

[22] R. G. Ellis, S. A. Coon, and B. H. J. McKellar, Nucl. Phys. **A438**, 631 (1985); S. A. Coon and M. T. Peña, Phys. Rev. C **48**, 2559 (1993); A. Stadler, J. Adam, H. Henning, and P. U. Sauer, Phys. Rev. C **51**, 2896 (1995).

[23] S. A. Coon, M. T. Peña, and D. O. Riska, Phys. Rev. C **52**, 2925 (1995).

[24] J. Adam, Jr., M. T. Peña, and A. Stadler, Phys. Rev. C **69**, 034008 (2004).
[25] M. Baldo and L. S. Ferreira, Phys. Rev. C **59**, 682 (1999).
[26] S. A. Coon and H. K. Han, Few-Body Syst. **30**, 131 (2001).
[27] J. L. Friar, D. Hüber, and U. van Kolck, Phys. Rev. C **59**, 53 (1999).
[28] S. A. Coon and M. D. Scadron, Phys. Rev. C **23**, 1150 (1981).
[29] J. Fujita and H. Miyazawa, Prog. Theor. Phys. **17**, 360 (1957).
[30] G. E. Brown and W. Weise, Phys. Rep. **22**, 279 (1975).
[31] E. Matsinos, W. S. Woolcock, G. C. Oades, G. Rasche, and A. Gashi, Nucl. Phys. **A778**, 95 (2006).
[32] Th. A. Rijken and V. G. J. Stoks, Phys. Rev. C **46**, 73, 102 (1992).
[33] B. K. Jain and A. B. Santra, Phys. Rep. **230**, 1 (1993).
[34] R. Machleidt (private communication).
[35] M. Soyeur, Nucl. Phys. **A671**, 532 (2000).
[36] M. T. Peña, D. O. Riska, and A. Stadler, Phys. Rev. C **60**, 045201 (1999).
[37] S. Huber and J. Aichelin, Nucl. Phys. **A573**, 587 (1994).
[38] S. Hirenzaki, P. Fernández de Córdoba, and E. Oset, Phys. Rev. C **53**, 277 (1996).
[39] B. Juliá-Díaz, A. Valcarce, P. González, and F. Fernández, Phys. Rev. C **66**, 024005 (2002).
[40] B. D. Day, Phys. Rev. C **24**, 1203 (1981); H. Q. Song, M. Baldo, G. Giansiracusa, and U. Lombardo, Phys. Rev. Lett. **81**, 1584 (1998); M. Baldo, G. Giansiracusa, U. Lombardo, and H. Q. Song, Phys. Lett. **B473**, 1 (2000); M. Baldo, A. Fiasconaro, H. Q. Song, G. Giansiracusa, and U. Lombardo, Phys. Rev. C **65**, 017303 (2001); R. Sartor, Phys. Rev. C **73**, 034307 (2006).
[41] T. Cheon and E. F. Redish, Phys. Rev. C **39**, 331 (1989); R. Sartor, Phys. Rev. C **54**, 809 (1996); K. Suzuki, R. Okamoto, M. Kohno, and S. Nagata, Nucl. Phys. **A665**, 92 (2000); F. Sammarruca, X. Meng, and E. J. Stephenson, Phys. Rev. C **62**, 014614 (2000).
[42] I. Bombaci and U. Lombardo, Phys. Rev. C **44**, 1892 (1991); M. Baldo, I. Bombaci, and G. F. Burgio, Astron. Astrophys. **328**, 274 (1997); H.-J. Schulze, A. Polls, A. Ramos, and I. Vidaña, Phys. Rev. C **73**, 058801 (2006).